Progress In Electromagnetics Research C, Vol. 114, 143–158, 2021

Multi-Resonator Variations of Circular Microstrip Antenna with Narrow Annular Sectoral Patches for Wideband Response

Venkata A. P. Chavali* and Amit A. Deshmukh

Abstract—Broadband variations of a proximity fed circular microstrip antenna gap-coupled with narrow annular sectoral patches are proposed. The gap-coupling of pairs of parasitic annular sectors along the x- and y-axes of the fed patch tunes the spacing in between the fundamental modes on the respective patches that yields wider bandwidth. A maximum bandwidth of 728 MHz (55%) offering peak gain of nearly 9 dBi is obtained in the circular patch gap-coupled with four pairs of annular sectors along the x-axis. This bandwidth is around 13% larger than the bandwidth offered by a single circular microstrip antenna. Instead of using multiple sectoral patches, a gap-coupled design of circular patch with a stub loaded annular sectoral patch is presented. The stub tunes its TM_{02} mode frequency with reference to the fundamental modes on the circular and sectoral patches that yields bandwidth of 660 MHz (51%). Resonant length formulation and subsequent design methodology for all the proposed gap-coupled configurations are presented, which helps in the re-designing of similar antennas at the given fundamental mode frequency. All the optimum and redesigned antennas are fabricated, and the measured results shows a close agreement with the simulations.

1. INTRODUCTION

The bandwidth (BW) of a microstrip antenna (MSA) can be increased by creating additional resonances near the fundamental resonant mode of the fed patch. Additional resonances can be realized by cutting slots at specific locations in the patch [1–5] or by incorporating parasitic patches [6–12]. In slot cut MSAs, the slot position governs which higher order mode contributes to the BW enhancement. This technique although yields low profile structures, but they are complex in designing. On the other hand, gap-coupled configurations are simpler and also result in increased gain due to larger aperture size. Additional patches can be incorporated on the same plane as that of the fed patch (planar multi resonator configurations) [13–23], or they can be placed above the fed patch (stacked configurations) [24–29]. In comparison with the planar configurations, stacked configurations result in an increased cross polarization radiation due to the volume enhancement in terms of total substrate thickness. So far, many configurations utilizing planar gap-coupling methods of regular shapes such as rectangle, triangle, and circle are reported. In the gap-coupled configurations, the shape of the parasitic patch decides the amount of gap-coupling and thus the BW. The planar configuration using a circular MSA (CMSA) gap-coupled with parasitic circular patches [6] exhibited less BW due to the curved circumference of the CMSA. Also, the gap-coupled configurations [11, 13, 18, 25] occupied larger area as the parasitic patch dimensions were comparable with that of the fed patch. Hence, the space around the fed MSA should be utilized in such a way that maximum coupling takes place between the fed and parasitic patches, resulting in an optimum BW without much increase in the overall patch size.

This paper presents a simpler and novel broadband variations of proximity fed CMSA gap-coupled with narrow annular sectoral patches, which are placed around the empty area adjoining the fed patch.

Received 16 June 2021, Accepted 28 July 2021, Scheduled 5 August 2021
* Corresponding author: Venkata A. P. Chavali (cpriyag@gmail.com).
The authors are with the EXTC Department, SVKM's DJSCE, Mumbai, India.

Thus, additional resonant modes are introduced without much increment in the total patch size. Initially, a proximity fed CMSA is optimized for the BW at the fundamental mode frequency of 1200 MHz. Further, annular sectoral patches are gap-coupled to the fed patch either along x-axis, or y-axis, or along both the coordinate axes. With the gradual addition of pairs of annular sectors, the number of resonant modes in the gap-coupled design increases that increases the MSA BW. With the parasitic patches along the x-axis, the design with four sectors yields the maximum BW of 694 MHz (52.2%) for reflection coefficient (S_{11}) less than -10 dB, offering peak gain of nearly 9 dBi. For the design along the y-axis, the maximum BW of 681 MHz (51.7%), using three annular sectors and a BW of 671 MHz (51.3%) with three pairs of sectoral patches along both the coordinate axes, is obtained. Both these optimum designs yield broadside gain of around 8.7 dBi with a broadside radiation pattern. Instead of adding more resonant modes using pairs of sectoral patches, the design of stub loaded single pair of annular sectors gap-coupled with proximity fed CMSA is presented. The stub tunes TM_{02} mode frequency on the sectoral patches with reference to the TM_{11} and TM_{01} modes which achieves an impedance BW of around 617 MHz ($\sim$ 48%). Based upon the optimum configurations, resonant length formulation and subsequent design methodology for the similar gap-coupled antennas at different frequencies are presented, which yields a similar wideband response. Wideband antennas using slots are complex to optimize as the slots are present inside the patch that affects the impedance variation across various resonant modes, whereas using multiple parasitic patches of nearly the same dimensions, the total patch size increases. Against these, the proposed configurations adds resonant modes using patches residing in the adjoining area of the fed patch, hence they are simpler in design and do not increase the patch size by a larger extent. This is the main technical novelty in the proposed work. A detailed comparison highlighting the same is presented further in the paper. The proposed configurations are initially optimized using CST software [31] followed by the experimentation using high frequency instruments namely, ZVH-8, FSC 6, and SMB 100 A, on a square ground plane of sidelength 35 cm. A close agreement is obtained between the simulated and measured results.

2. CMSA GAP-COUPLED WITH NARROW PARASITIC ANNULAR SECTORAL MSAS

Broadband designs of proximity fed CMSA gap-coupled with narrow annular sectoral MSAs are shown in Figs. 1(a)–(d). The patch dimensions and frequencies referred in the paper are in 'cm' and 'MHz', respectively.

To ensure the optimum coupling between the fed and parasitic patches, besides an optimum space utilization, here narrow annular sectors are gap-coupled with the fed CMSA. The fundamental mode currents 'J_x' and 'J_y' on each pair of parasitic sectors for the three variations of proximity feed positions are shown in Fig. 1(c). For the gap-coupled configuration in which annular sectors are placed along the x-axis, if the feed point is chosen along x-axis, i.e., at 'F_1', then maximum of CMSA's TM_{11} resonant field gets coupled with the minimum of the fundamental mode fields on the annular sectors, which results in no coupling of energy from the fed CMSA to the parasitic annular sectors. Similarly, for the annular sectors gap-coupled along y-axis, with the proximity feed strip at 'F_2', results in zero energy excitation in the parasitic patches. Hence, to increase the gap-coupling between the fundamental modes of the CMSA and annular sectors, a common proximity feed location is chosen, along the offset position, i.e., at 'F_3'. In all the designs, initially CMSA is designed for the fundamental TM_{11} mode frequency of 1200 MHz. The CMSA is designed on an FR4 substrate ($\varepsilon_r = 4.3$, $h = 0.16$, $\tan\delta = 0.02$) which is suspended above the ground plane using an air gap of 'h_a' = 2.4 cm, making the total substrate thickness '$h + h_a$' = 2.56 cm ($\sim 0.1\lambda_g$). The CMSA radius 'R' is calculated using the reported resonance frequency equation [1] followed by the parametric optimization on thicker substrate. The value of 'R' is found to be 5 cm. A square proximity strip of dimensions 'l_s' = 1.4 cm is placed below the patch at 'h_s' = 2.2 cm, located at $(x_f, y_f) = (1.8, 1.8)$ cm. This CMSA yields the simulated BW of 520 MHz (4%) with a peak broadside gain of 8.9 dBi. Further, in the gap-coupled designs, broadband behavior is studied by placing one pair of annular sectors along the x-axis. The BW enhancement is attained by optimizing the gap between the fed and parasitic patches, radius, and angle of the annular sectors, which decides the TM_{01} mode frequency of the individual sector. The optimization of antenna results in space tuning between the fundamental modes of the fed and parasitic patches. Gradually, the number of pairs

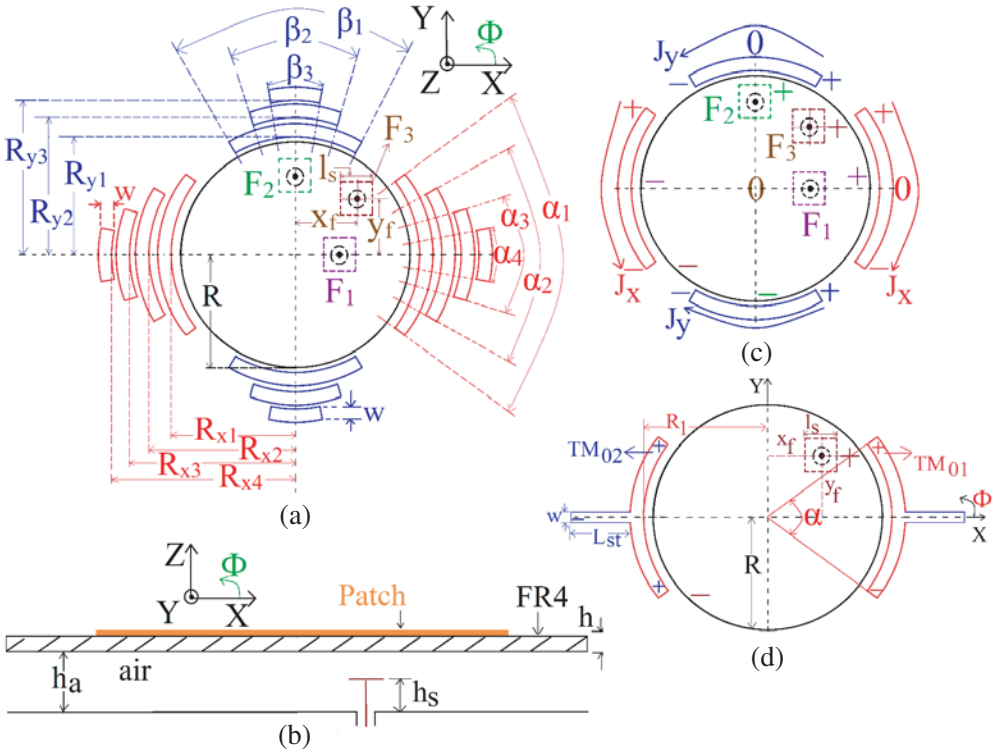

Figure 1. CMSA gap-coupled with parasitic annular sectoral patches; (a) top and (b) side views, (c) field and modal current directions for different feed strip locations and, (d) CMSA gap-coupled with stub loaded pair of annular sectoral MSAs.

of annular sectors is increased to enhance the BW. A similar study is carried out by placing annular sectors along y-axis and along both x- and y-axes. In the stub loaded variation, using the parametric optimization for the stub length increments that tunes its TM_{02} mode frequency, an optimization of the BW is achieved as explained in the following sections.

3. PROXIMITY FED CMSA GAP-COUPLED WITH ANNULAR SECTORS ALONG X-AXIS AND Y-AXIS

To increase the BW, initially one pair of annular sectors is gap-coupled along the x-axis as shown in Fig. 1(a). The sectoral angle 'α_1' and radius 'R_{x1}' of the annular sectors are optimized parametrically to achieve the increase in the BW. From the surface current distributions observed at the resonance peaks, the mode in annular sector is identified as TM_{01} as shown with the currents 'J_x' in Figs. 1(c) & 2(b). For 'R_{x1}' = 5.5 cm and 'α_1' = 70, a simulated BW of 639 MHz (48.8%) with a peak gain of 8.8 dBi is obtained. Further enhancement in the BW is achieved by adding additional pairs of annular sectors along the x-axis. The addition of pairs of sectoral patches adds to higher number of resonant modes near the TM_{11} mode of the fed patch that increases the BW. A smaller improvement in the gain characteristics is also observed due to the additional parasitic patches. In each design, sectoral patch angle and parasitic annular sectors' radius and position (gap spacing) are parametrically optimized. A maximum BW is obtained in CMSA gap-coupled with four pairs of annular sectors along the x-axis with dimensions, 'R_{x1}' = 5.2, 'R_{x2}' = 6.3, 'R_{x3}' = 7.4, 'R_{x4}' = 8.4, 'w' = 0.8, 'α_1' = 70, 'α_2' = 60, 'α_3' = 40, 'α_4' = 20, $(x_f, y_f) = (2.5, 2.5)$, 'l_s' = 1.4 cm. The variation in gain, simulated and measured BWs, and % increment in the area with respect to number of pairs of annular sectoral patches is shown in Fig. 2(a). With an increment in the number of annular sector pairs, an enhancement in the BW is observed. Using four pairs, an optimum simulated BW of 694 MHz (52.2%) and a measured BW of 728 MHz (55%) with a peak gain of nearly 9 dBi are obtained as shown in Fig. 2(c). This BW is

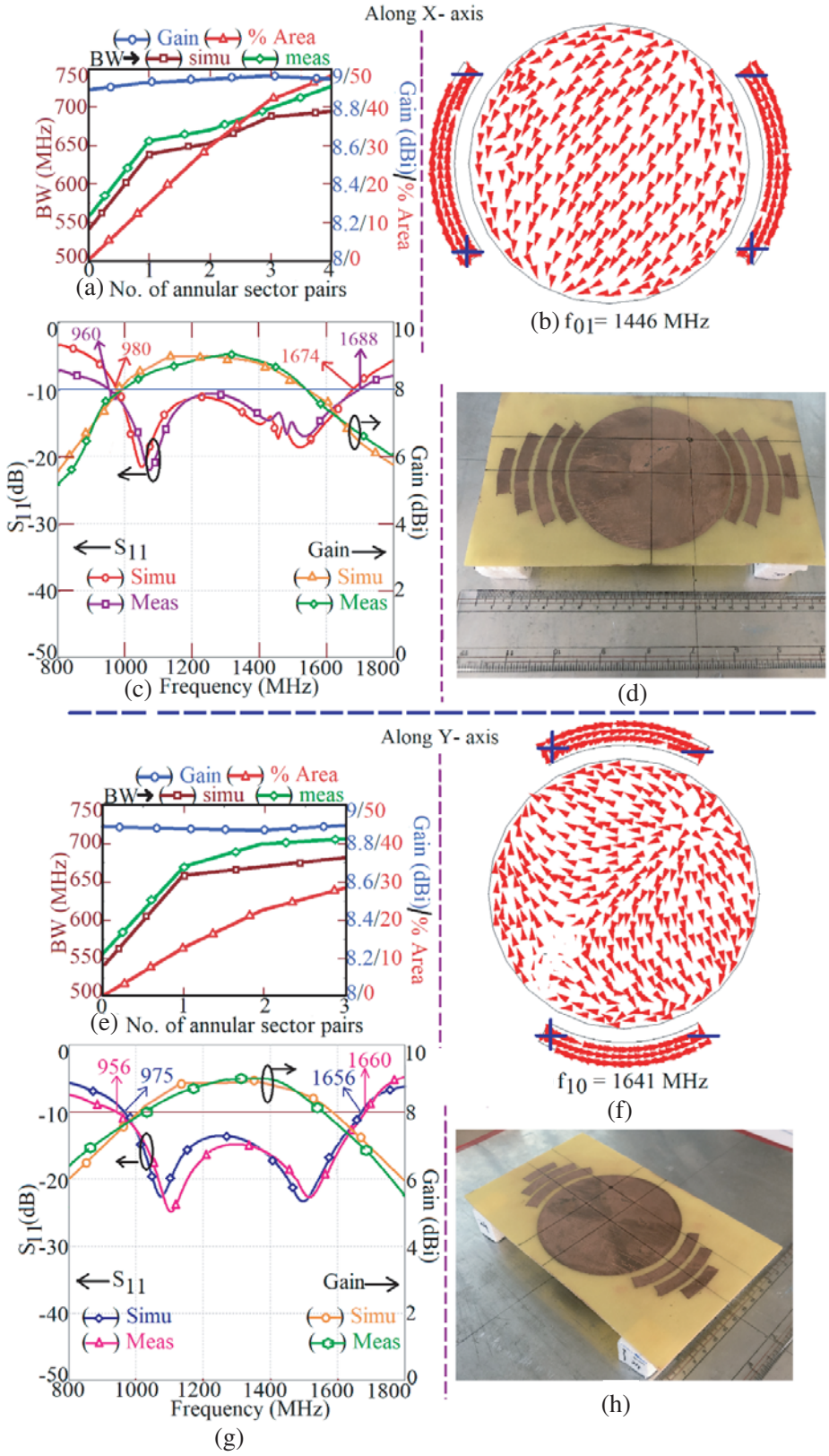

Figure 2. Antenna parameters against number of annular sectors, their optimum results, modal current plots and fabricated prototypes for CMSA gap-coupled along (a)–(d) x-axis and (e)–(h) y-axis.

around 13% larger than that of a single CMSA. The area increment is around 46%, which is smaller than those using a conventional half wavelength resonator offering equivalent BW. Slight decrease in the gain for CMSA gap-coupled with four pairs of annular sectors is observed due to the asymmetry in the configuration leading to a smaller component of the orthogonal modal currents on the patch. This asymmetry is due to the parasitic patches present only along the x-axis. The fabricated prototype of CMSA with four pairs of annular sectors along x-axis is shown in Fig. 2(d).

Similarly, CMSA gap-coupled with parasitic annular sectors along y-axis is studied for the BW increment. The annular sector angle 'β_1' and radius 'R_{y1}' are parametrically optimized to get an increase in the BW. From the surface current distributions, the resonant mode on the parasitic sector is identified to be TM_{10} as the surface currents are aligned along the horizontal directions as shown with 'J_y' in Fig. 1(c) and Fig. 2(f). Due to the space tuning between TM_{11} mode of CMSA and TM_{10} modes of single pair of annular sectors, a simulated BW of 660 MHz (49.9%) is realized with a gain of 8.9 dBi.

With a gradual inclusion of the additional pairs of annular sectors, the BW improves further. The variation in gain, simulated and measured BWs, and % increment in the area with respect to the number of pairs of annular sectoral patches is shown in Fig. 2(e). Using parametric optimization, maximum BW is obtained for CMSA gap-coupled with three pairs of annular sectors with dimensions; 'R_{y1}' = 5.5, 'R_{y2}' = 6.6, 'R_{y3}' = 7.7, 'w' = 0.8, 'β_1' = 60, 'β_2' = 40, 'β_3' = 20, $(x_f, y_f) = (2.5, 2.5)$, 'l_s' = 1.4 cm. Using three pairs of parasitic patches, a simulated BW is 681 MHz (51.76%), and the measured BW is 704 MHz (53.8%) showing peak broadside gain of 8.9 dBi, as shown in Fig. 2(g). The BW incremen about 13% is obtained in comparison with a CMSA. The fabricated prototype for three pairs of annular sectors along y-axis is shown in Fig. 2(h). The radiation pattern plots near the band start and stop frequencies for the CMSA gap-coupled with four pairs of annular sectors along x-axis are shown in Figs. 3(a)–(d). Since the diagonal feed position is present, E and H-planes are aligned along $\Phi = 45$ and 135, respectively. The pattern exhibits broadside radiation with higher cross polarization levels in the H-plane. This is attributed to the asymmetry in the H-plane of the MSA, due to the placement of annular sectors only along the x-axis. Similar pattern characteristics are observed for the gap-coupled

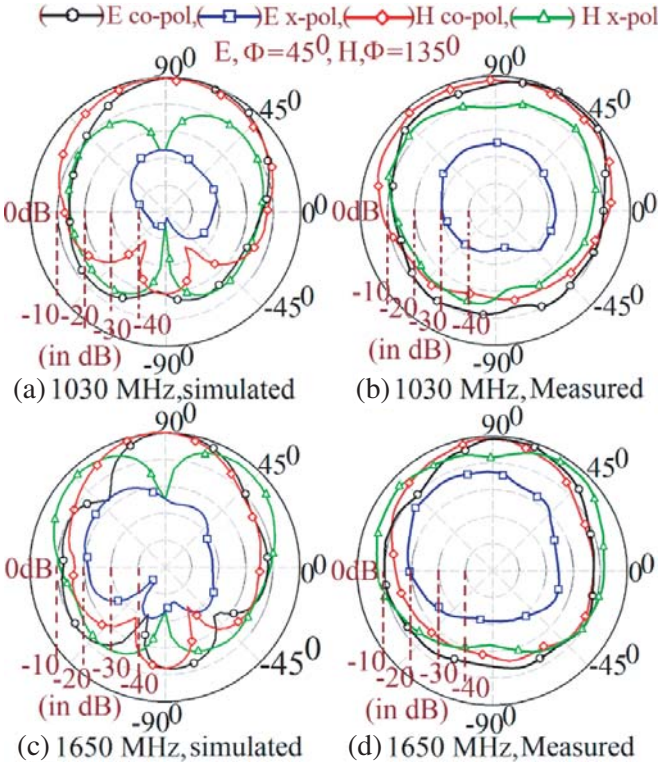

Figure 3. (a)–(d) Radiation pattern plots nearer to the band edge frequencies for the CMSA gap-coupled with annular sectoral patches along x-axis.

design along the y-axis.

An equivalent circuit of CMSA gap-coupled with one pair of annular sectors along the x-axis is shown in Fig. 4, which is drawn based on the transmission line equivalence of the MSA. Here, the fed patch and parasitic annular sectors are represented with respective parallel R-L-C circuits at the fundamental mode of resonance. The gap between the parasitic and fed patches is represented with 'π' network of capacitance, where 'C_c' represents the coupling between fed and parasitic patches, and 'C_g' shows the effect of electric field distribution at the open edges of the fed patch. With the addition of parasitic sectors, additional gap equivalent and parallel R-L-C circuits are added. Towards the end, the circuit is loaded with parallel combination of R and C, representing the radiation and stored energy from the slots.

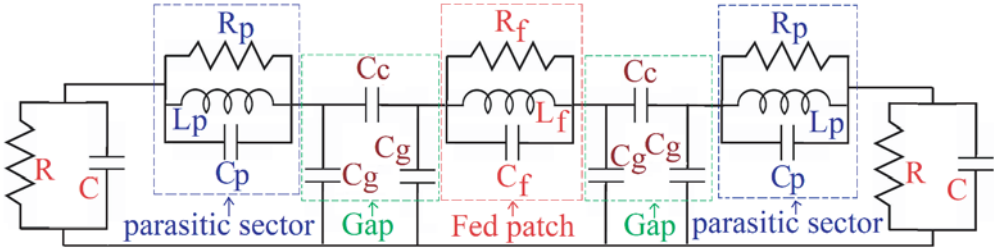

Figure 4. Equivalent circuit of CMSA with one pair of annular sectors along x-axis.

Radiation pattern and gain measurement setup are shown in Fig. 5(a). A distance of more than '$2D^2/\lambda$' is kept between the reference wideband Horn antenna and the antenna under test (AUT). Measurement was carried out inside an antenna lab, where minimum reflections from the surrounding objects was ensured at the measurement frequency. Using the three antenna method, broadside antenna gain is measured.

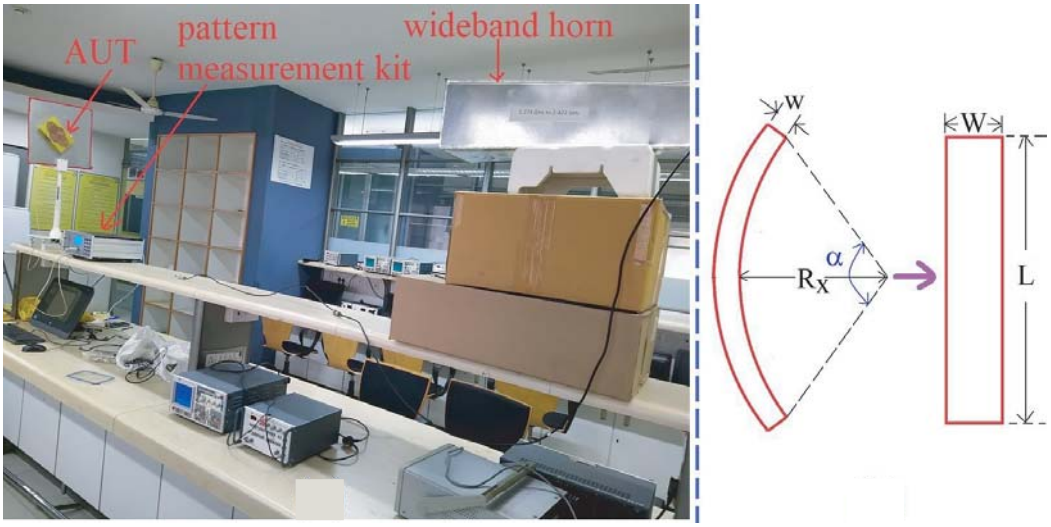

(a) (b)

Figure 5. (a) Measurement setup for the CMSA gap-coupled with pairs of annular sectors, (b) equivalence between annular sectoral and rectangular patch.

Based on the optimum configuration at 1200 MHz, design procedure for the CMSA gap-coupled with four pairs of annular sectors along x-axis and CMSA gap-coupled with three pairs of annular sectors along y-axis at the given fundamental frequency is proposed. Initially, the effective dielectric constant 'ε_{re}' of the suspended dielectric substrate is chosen to be 1.05. This value is chosen based

upon the value of 'ε_{re}' in the optimum configuration at 1200 MHz. The total dielectric thickness in the suspended substrate ('$h_t = h_a + h$') is chosen to be $0.1\lambda_g$. With respect to this total substrate thickness, practically realizable value of air gap 'h_a' is chosen. Based upon the new value of 'h_a', effective dielectric constant value is recalculated using series capacitance equation [1]. The radius 'R' of the CMSA for the TM_{11} mode on thicker substrate is calculated using Equations (1) and (2). The multiplying factor of 0.5 for the fringing field extension length is selected based upon the parametric study of CMSA at different frequencies and substrate thicknesses. The radius values of the parasitic annular sectors and their width 'w' are chosen based upon the ratios of 'R/R_{x1}', 'R/R_{x2}', 'R/R_{x3}', 'R/R_{x4}' and 'w/R' as present in the original optimum configuration along x-axis at 1200 MHz. Similarly, values of 'R/R_{y1}', 'R/R_{y2}', 'R/R_{y3}' for the MSA gap-coupled along y-axis are calculated. The angles of annular sector pairs (α_1, α_2, α_3, α_4 for annular sectors along x-axis and β_1, β_2, β_3 for annular sectors along y-axis) are chosen to be the same as that in the optimum configuration at 1200 MHz. Thus, the angles are selected as 70°, 60°, 40°, and 20° for annular sectors pairs along x-axis and 60°, 40°, and 20° for annular sectors pairs along y-axis. The resonant frequency equations for the annular sectoral patches in the gap-coupled configurations are proposed with the help of their area equations. The area of annular sectors is calculated by using Equation (3) for CMSA gap-coupled along x-axis and by using Equation (4) for CMSA gap-coupled along y-axis.

$$R_e = K_{nm}C/2\pi f_{11}\sqrt{\varepsilon}_{re} \tag{1}$$

$$R = R_e\left(2 \times 0.5 \times h_t/\sqrt{\varepsilon}_{re}\right) \tag{2}$$

where, $K_{nm} = 1.84118$ for TM_{11} mode

$$A_{xi} = (\pi/360)\,\alpha_i\left((R_{xi}+w)^2 - (R_{xi})^2\right) \tag{3}$$

$$A_{yi} = (\pi/360)\,\beta_i\left((R_{yi}+w)^2 - (R_{yi})^2\right) \tag{4}$$

$$L = A_{xi}/w \tag{5}$$

$$L = A_{yi}/w \tag{6}$$

where $i = 1, 2, 3, 4$, '$R_{xi} + w$' or '$R_{yi} + w$' — outer radius of ith annular sector pair, 'w' — width of annular sector pairs.

$$L_{eff} = L + \Delta L \tag{7}$$

$$\Delta L = 2 \times 0.7\ (h_t)/\sqrt{\varepsilon_{re}} \tag{8}$$

$$f_{01} = C/\left(2L_{eff}\sqrt{\varepsilon_{re}}\right) \tag{9}$$

$$f_{10} = C/\left(2L_{eff}\sqrt{\varepsilon_{re}}\right) \tag{10}$$

Based on the values of the area as calculated using Equations (3) & (4) and the width 'w' of the annular sector pairs, equivalent length 'L' of annular sectors can be calculated by using Equation (5) for CMSA gap-coupled along x-axis and using Equation (6) for CMSA gap-coupled along y-axis. This is done to establish the equivalence between the annular sector and rectangular patch of length 'w' and width 'L' as shown in Fig. 5(b). Thus, resonance frequency of TM_{01} mode of the annular sector along x-axis is calculated by using Equations (5) and (7)–(9). The resonance frequency for TM_{10} mode of annular sector along y-axis is calculated by using Equations (6)–(8) and (10). Here 'C' is the velocity of light in free space, and 'ΔL' accounts for the fringing field extension length. Based upon the parametric study at different frequencies and substrate thicknesses, the fringing field length multiplying factor of '0.7' is chosen. The feeding strip parameters, position 'x_f', length 'l_s', and its location below the fed patch 'h_s', are chosen as '$0.5R$', '$0.06\lambda_g$' and '$0.09\lambda_g$', respectively.

Using the above procedure, CMSA gap-coupled with annular sector pairs along x-axis and y-axis are designed at 2000 MHz. The variation in gain, simulated and measured BWs and % increment in the area with respect to the increment in number of pairs of annular sectors is shown in Fig. 6(a). The dimensions obtained using proposed redesign methodology for the gap-coupled design along x-axis using four pairs of sectoral patches are: 'R_{x1}' = 2.6, 'R_{x2}' = 3.15, 'R_{x3}' = 3.7, 'R_{x4}' = 4.2, $(x_f, y_f) = (1.25, 1.25)$, '$l_s$' = 0.85, '$h_s$' = 1.3 cm. For these parameters, frequencies observed in the simulation of the annular sectors match closely with those calculated by using Equations (9) and (10). The simulated BW is 1489 MHz (59.4%) whereas the measured BW is 1504 MHz (59.9%), offering 7.2 dBi

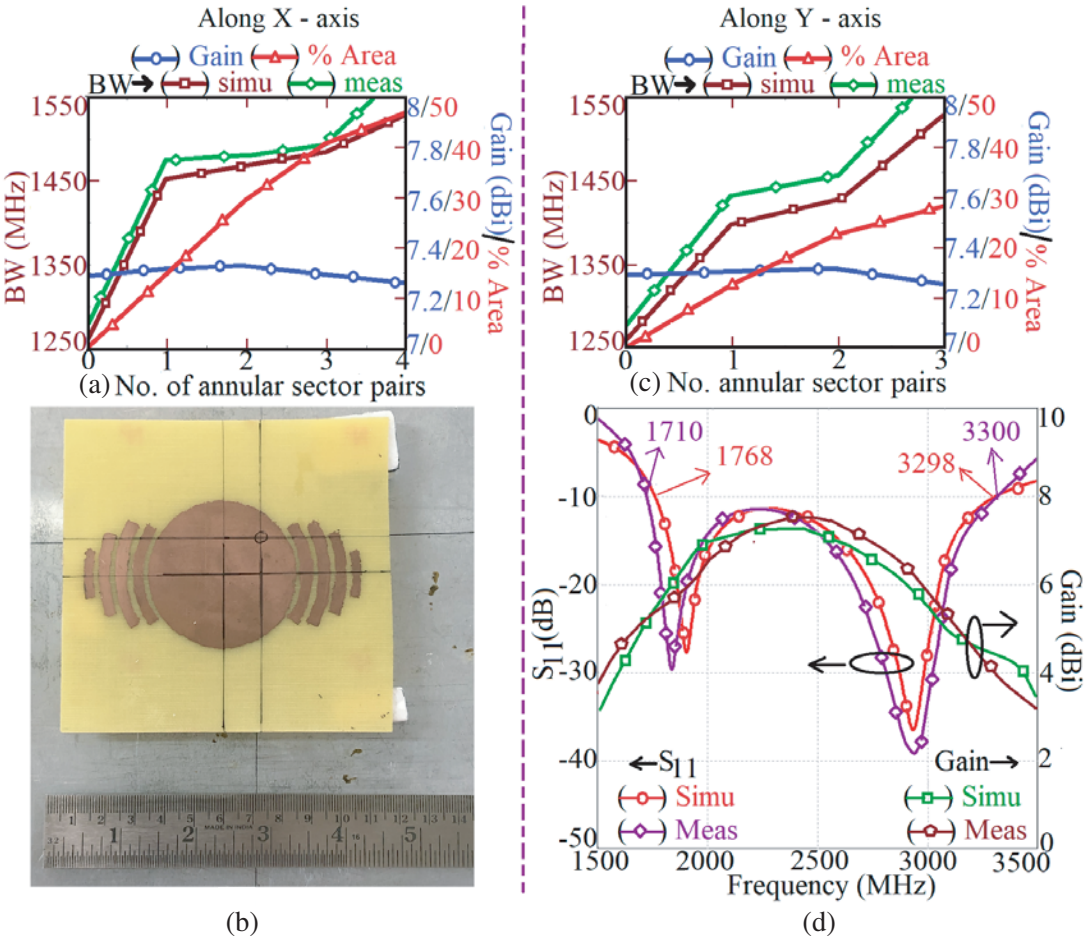

Figure 6. Antenna parameters against number of pairs of annular sectors, their optimum results and fabricated prototypes for CMSA gap-coupled with annular sectors along (a), (b) x-axis, (c), (d) y-axis at $f_{TM11} = 2000$ MHz.

of the peak gain. The fabricated prototype of CMSA with gap-coupled sector pairs along the x-axis is shown in Fig. 6(b). Further, the dimensions obtained using proposed redesign methodology for the CMSA gap-coupled with three pairs of annular sectors along y-axis are: 'R_{y1}' = 2.75, 'R_{y2}' = 3.3, 'R_{y3}' = 3.85, $(x_f, y_f) = (1.25, 1.25)$, '$l_s$' = 0.85 cm. The variation in gain, simulated and measured BWs, and % increment in area with respect to the increase in number of annular sectors is shown in Fig. 6(c). Here the simulated BW of 1530 MHz (60.4%) and measured BW of 1590 MHz (63.47%), with a peak gain of 7.26 dBi, are realized as shown in Fig. 6(d).

4. PROXIMITY FED CMSA GAP-COUPLED WITH ANNULAR SECTORS ALONG BOTH THE COORDINATE AXIS

Both the gap-coupled configurations of CMSA discussed above are asymmetrical, as annular sectors are present along either x- or y-axis. Symmetry can be achieved by gap coupling the CMSA with narrow annular sectors along both the axes as shown in Fig. 1(a). By the gradual addition of the pairs of annular sectors along both the axes, tuning of the fundamental TM_{01} and TM_{10} modes of annular sectors takes place with respect to the TM_{11} mode. The radius values and angles of annular sectors considered in this composite configuration are similar to the values as in their individual designs along x- and y-axes. As the area of annular sector along x-axis is larger than the annular sectors along y-axis, the first mode near TM_{11} mode of CMSA is TM_{01} mode of the annular sectors gap-coupled along x-axis

followed by the TM_{10} mode of the sectors along y-axis. With one pair of annular sectors along x-y axis, a simulated BW of 633 MHz (48%) is achieved with a peak gain 9 dBi. Further enhancement in the BW is achieved by gradually increasing the number of pairs of annular sectors. The variation in gain, simulated and measured BWs, and % increment in the area with respect to the number of annular sector pairs is shown in Fig. 7(a). A maximum simulated and measured BWs of 652 MHz (50.23%) and 708 MHz (55%), respectively, are observed in CMSA gap-coupled with three pairs of sectors,showing peak gain around 9.1 dBi, as given in Fig. 7(b). This BW is nearly 12% higher than that given by single CMSA. Over the entire BW, broadside radiation pattern is observed. The E- and H-planes are aligned along $\Phi = 45$ and 135, respectively. The fabricated prototype of the antenna is shown in Fig. 7(c).

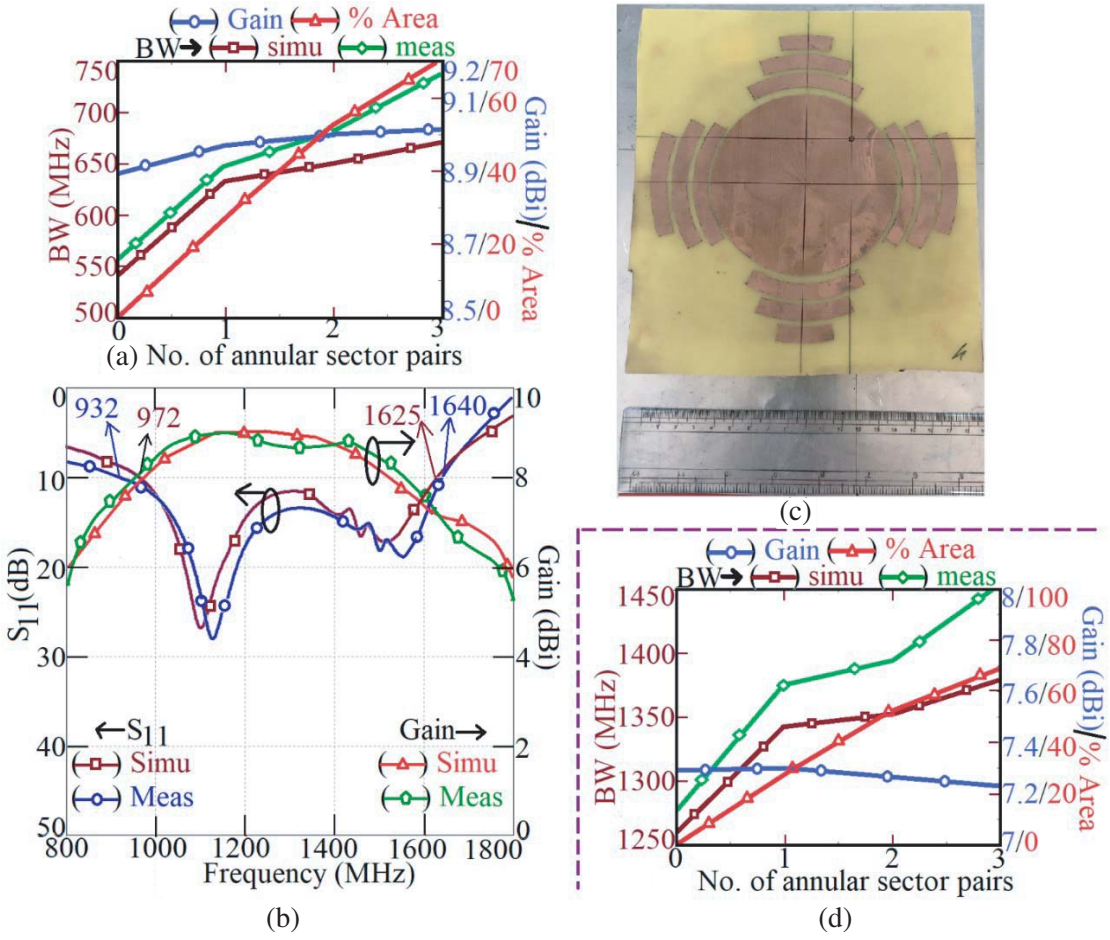

Figure 7. Antenna parameters against number of pairs of annular sectors, optimum results and fabricated prototype for CMSA gap-coupled with annular sectors along x and y-axes at f_{TM11} = (a)–(c) 1200 MHz, (d) 2000 MHz.

Based on the optimum configuration proposed at 1200 MHz, redesign procedure for CMSA gap-coupled with three pairs of annular sectors along x- and y-axes is proposed. A combination of the design procedure of CMSA gap-coupled with three pairs of annular sectors along each x-axis and y-axis is adopted here. The procedure for calculating 'ε_{re}', 'h_a', and other dimensions, such as CMSA radius, sector angles, feeding strip dimensions, feed position, and spacing between sectors, is same as that of the procedure as employed in CMSA gap-coupled with three pairs of sectors along the two axes. Using this procedure, the dimensions obtained for CMSA gap-coupled with three pairs of annular sectors along x and y-axis at 2000 MHz are: 'R_{x1}' = 2.6, 'R_{x2}' = 3.15, 'R_{x3}' = 3.7, 'α_1' = 70, 'α_2' = 60, 'α_3' = 40 and 'R_{y1}' = 2.75, 'R_{y2}' = 3.3, 'R_{y3}' = 3.85, 'β_1' = 60, 'β_2' = 40, 'β_3' = 20, $(x_f, y_f) = (1.25, 1.25)$, '$l_s$'

= 0.85 cm. The variation in gain, simulated and measured BWs, and % increment in area with respect to the increase in number of annular sectors is shown in Fig. 7(d). For the maximum BW design, simulated BW of 1380 MHz (56%) and measured BW of 1456 MHz (59.4%) with a gain of 7.3 dBi are obtained. The radiation patterns observed over S_{11} BW is similar to the original configuration at 1200 MHz. For these gap-coupled designs, to add more resonant modes, additional sectors are needed. Instead of this, stub loaded design is considered which tunes higher order mode of the annular sectoral patches for the BW improvement, as discussed in following section.

5. CMSA GAP COUPLED WITH STUB LOADED ANNULAR SECTORS

Broadband variation of CMSA gap-coupled with stub loaded pair of annular sectors is shown in Fig. 1(d). Without the stub, resonant modes excited on the fed and parasitic patches are TM_{11} and TM_{01}. To alter the frequency of any resonant mode, slots are loaded at its maximum current location whereas the stubs are placed at maximum field location. Here, as the stub position is in the center of sector, it coincides with the maximum field position of TM_{02} mode, and thus the placement of stub tunes its frequency with respect to the fundamental TM_{11} mode of CMSA that results in enhanced BW. No significant effect is observed on the fundamental TM_{01} mode frequency of the annular sector, since the stub is placed near the maximum current location of the TM_{01} mode. Thus, the stub length is

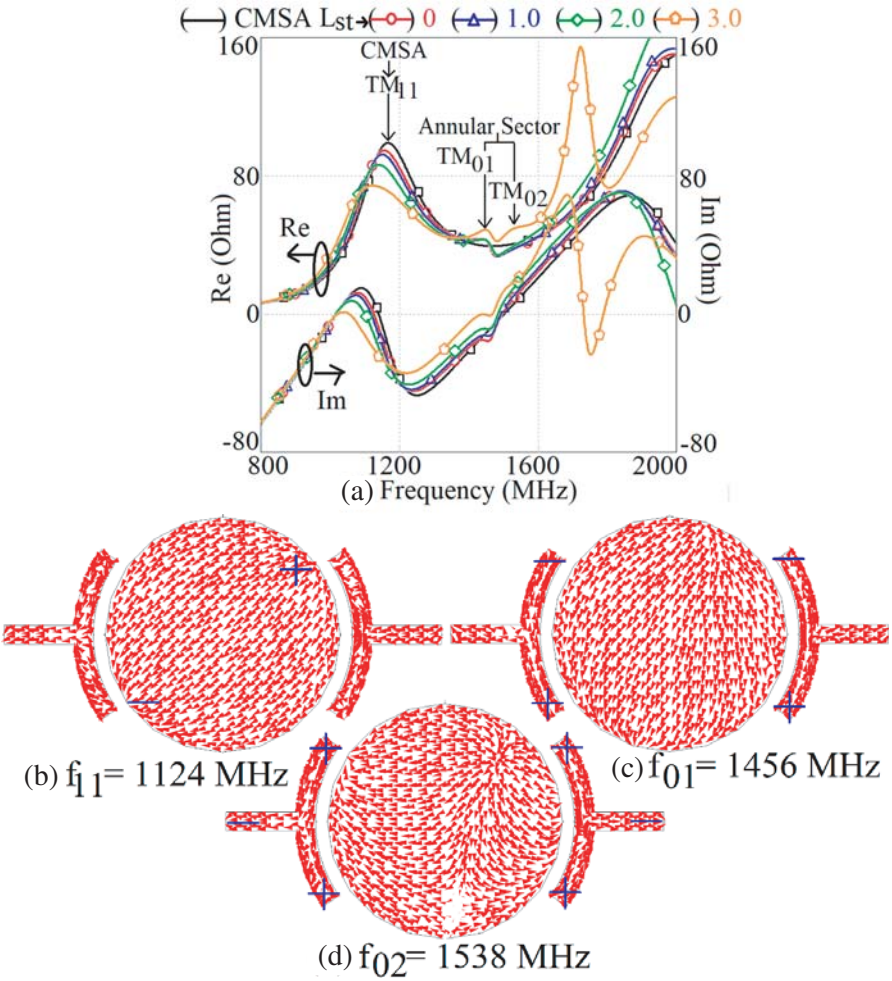

Figure 8. (a) Resonance curve plots for different stub lengths, and (b)–(d) surface current distributions at observed resonant modes for CMSA gap-coupled with stub loaded annular sectors optimized at 1200 MHz.

optimized as shown in Fig. 8(a) for the frequency tuning to yield a wider BW. The simulated surface current distributions at the observed resonant modes are shown in Figs. 8(b)–(d). Optimum result is obtained for 'L_{st}' = 3 cm, and its simulated and measured S_{11} and gain plots are shown in Fig. 9(a). The simulated BW is 617 MHz (47.95%) whereas the measured BW is 653 MHz (50.95%). The broadside peak antenna gain is 9.2 dBi. The pattern is in the broadside direction with E and H-planes aligned along $\Phi = 45$ and 135, respectively. The fabricated prototype of the stub loaded design is shown in Fig. 9(b). Due to the presence of TM_{02} mode towards higher frequencies of the BW, cross polarization level increases towards those frequencies.

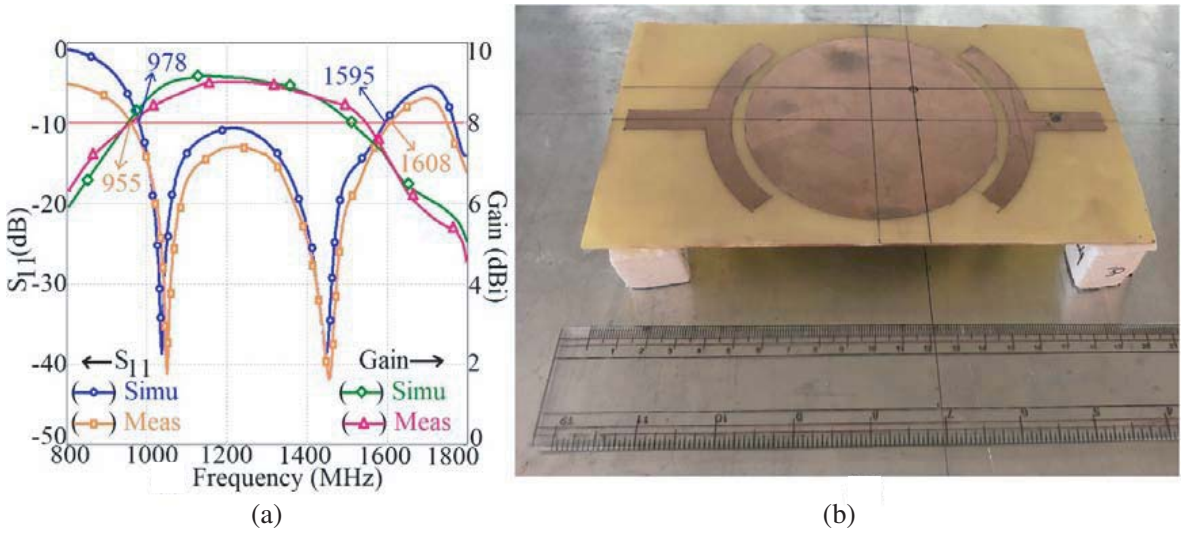

Figure 9. (a) S_{11} and gain plots, (b) fabricated prototype of CMSA gap-coupled with stub loaded annular sectors optimized at 1200 MHz.

Based on the optimum configuration of CMSA gap-coupled with stub loaded patches, a design methodology is presented here. Initially, the effective dielectric constant 'ε_{re}' of the suspended dielectric substrate is chosen to be 1.05. The total dielectric thickness of the suspended substrate ('$h_a + h$') is chosen to be $0.1\lambda_g$. For this total substrate thickness, practically a realizable value of 'h_a' is chosen. Based on new value of 'h_a', 'ε_{re}' value is recalculated. The CMSA radius 'R' for the given TM_{11} mode frequency is calculated using Equations (1) and (2). The radius of the annular sector is selected based upon the ratio of 'R/R_{x1}' as in the optimum configuration at 1200 MHz. The angle of annular sector pair 'α' is chosen to be the same as that in the optimum configuration, i.e., 70. The total area of the stub loaded annular sectors is calculated by using Equation (11). From this total area, effective length 'L' is calculated using Equation (12). This represents the equivalence of stub loaded annular sectoral patch with the equivalent rectangular patch. Further, the resonance frequency for TM_{02} mode of the annular sector pair is calculated using Equations (13)–(15). With reference to the stub loaded configuration at 1200 MHz discussed above, the proximity feeding strip dimension ('l_s') and length of the stub ('L_{st}') are expressed in terms of the wavelength 'λ_g' of the TM_{11} mode. The position of the feed is expressed as 'x_f/R' as observed from the ratio in the optimum design above. Using this procedure CMSA gap-coupled with stub loaded annular sectors is designed at $f_{TM11} = 2000$ MHz. The dimensions obtained are: 'R_1' = 2.75, 'L_{st}' = 1.85, $(x_f, y_f) = (1.15, 1.15)$ cm. The simulated BW here is 1070 MHz (46.7%) whereas the measured value is 1131 MHz (49.4%), with 7.1 dBi of peak gain as shown in Fig. 10(a). The fabricated prototype of stub loaded redesigned antenna is shown in Fig. 10(b).

$$A = \frac{\pi}{360}\alpha\left((R_{x1}+w)^2 - R_{x1}^2\right) + (L_{st} \times w) \tag{11}$$

where L_{st} = stub length, w = width of stub & width of annular sectoral patch.

$$L = A/w \tag{12}$$

$$L_{eff} = L + \Delta L \tag{13}$$

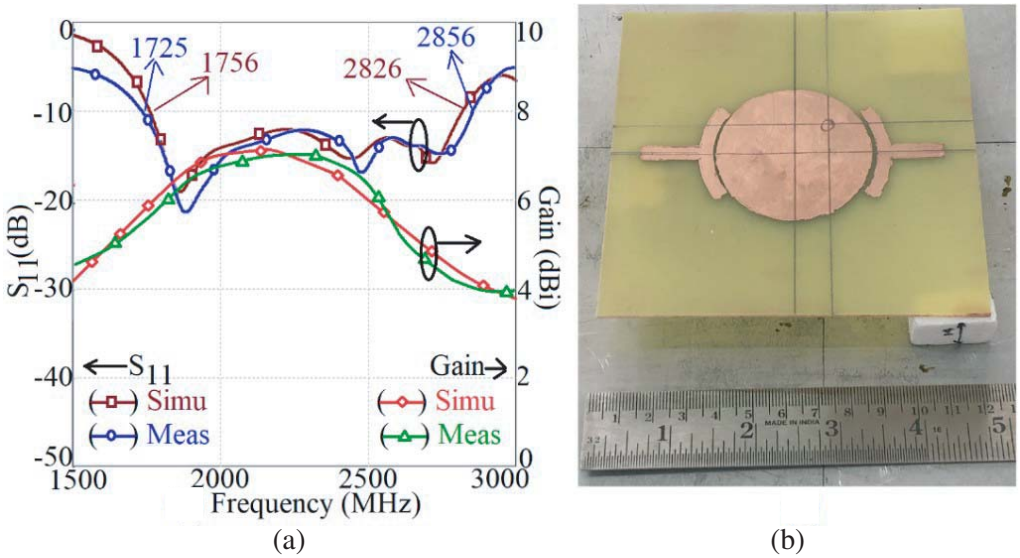

Figure 10. (a) S_{11} and gain plots and (b) fabricated prototype of CMSA gap-coupled with stub loaded annular sectors at 2000 MHz.

$$\Delta L = 2 \times 1.789 \ (h_a + h) / \sqrt{\varepsilon_{re}} \tag{14}$$

$$f_{02} = C / (L_{eff} \sqrt{\varepsilon_{re}}) \tag{15}$$

Using the resonance frequency equations as proposed for the annular sectoral patches, a comparison of the calculated values against simulated frequencies for various CMSA gap-coupled configurations is provided in Table 1. The % error between the simulated and calculated values obtained using Equation (16) is less than 5% in each case, thereby validating the propose formulations.

$$\%error = [|f_{sim} - f_{cal}| / f_{sim}] \times 100 \tag{16}$$

Of the many techniques reported for the BW improvement in MSA, the multi-resonator gap-coupled technique is the simplest one. In the reported papers, many configurations using this method have been presented, but those designs either employ conventional half wavelength resonator or reduce

Table 1. Comparison of simulated and calculated frequencies of the redesigned CMSA gap-coupled configurations.

MSA shown in	Annular sector pair	Resonant Mode	f_{sim} (MHz)	f_{cal} (MHz)	% error
Fig. 1(a), sectors along x-axis	–	f_{11}	2050	2000	2.43
	1	Arc1 $- f_{01}$	2570	2520	1.95
	2	Arc2 $- f_{01}$	2720	2730	0.36
Fig. 1(a), sectors along y-axis	–	f_{11}	2050	2000	2.44
	1	Arc1 $- f_{10}$	2897	3000	3.55
Fig. 1(a), sectors along x-y axis	–	f_{11}	2040	2000	1.96
	1	X-arc1 $- f_{01}$	2560	2520	1.56
	2	X-arc2 $- f_{01}$	2734	2730	0.14
	3	Y-arc1 $- f_{10}$	2882	3000	4.09
CMSA gap-coupled with stub loaded annular sectors	–	f_{11}	1920	2000	4.16
	Stub	f_{02}	2576	2660	3.26

size variation of the regular shape patch or employ modified patch shapes, which does not function around the fundamental patch mode. In the present work along with the fed patch of half wavelength in dimension, compact modified shapes geometries which are half wavelength in dimensions are gap-coupled in an empty area around the fed patch to enhance the BW, thereby resulting in a smaller area increment. Thus, to highlight the novelty in the proposed work against the reported configurations, a detailed comparison is presented in Table 2. For the comparison purpose, patch area and substrate thickness are normalized with respect to guided wavelength (λ_c) at the centre frequency of the BW. Amongst all the proposed designs, gap-coupled design along x-axis yields the maximum BW and gain. Hence, this configuration is selected for the comparison purpose. A compact wideband gap-coupled antenna with three staggered patches is reported in [7]. Here a stable radiation pattern with low cross-polarization is reported. However, the BW achieved is 6.8% which is very much less than the BW realized by the proposed design. Also, the explanations regarding the resonant modes responsible for the enhanced BW with respect to the feed location are missing. A high gain wideband MSA gap-coupled with mushroom type structures reported in [9] realized slightly increased gain with comparable substrate thickness. However, this gap-coupled design requires shorting post to be placed in the gap-coupled mushroom cells. The planar gap-coupled MSAs in [10, 11] offers narrow BW. Due to the increased patch area, although a larger gain is realized by the MSAs reported in [11, 14], the BW realized is narrow. Similarly, although compact configurations with respect to the substrate thickness are reported in [12, 14, 15, 19], the BW achieved is smaller. The stacked gap-coupled triangular and elliptical patches discussed in [25, 26] exhibit similar BW to the proposed design but have improved gain performances due to cavity backed design. However, this cavity-backed approach increases the design complexity. Also, the stacked plus gap-coupled configuration increases the antenna size and volume. The peak gain

Table 2. Comparison of proposed CMSA gap-coupled variation against reported designs.

MSA shown in	BW enhancement technique	Meas. BW (%)	Peak Gain (dBi)	Patch area A/λ_c	Substrate thickness h/λ_c
Fig. 1(a), sectors along x-axis	**Gap-coupled**	**55**	**9**	**5.2**	**0.115**
Ref. [7]	Staggered gap coupled	6.8	7	0.741	0.04
Ref. [9]	Gap coupled shorted patches	40	10	1.354	0.113
Ref. [10]	Gap coupled with slot	27.3	6.4	1.62	0.152
Ref. [11]	Gap coupled	12.3	12	11.37	0.104
Ref. [12], Circular sector with parasitic ring	Gap coupled	5.75	–	5.29	0.074
Ref. [12], Annular ring with shorting pin	Gap coupled with shorting pin	6.3	–	8.27	0.071
Ref. [13]	Gap coupled with slot	26.2	8.5	2.78	0.115
Ref. [14]	Shorted edges	13.2	9.7	2.84	0.054
Ref. [15]	Gap coupled	10.5	–	1.111	0.039
Ref. [19]	Gap coupled shorted patches	13.8	5	2.371	0.067
Ref. [25]	Stacked gap coupled	42.2	10.8	5.37	0.233
Ref. [26]	Stacked gap coupled	55.7	12.3	14.7	0.155
Ref. [29]	Stacked	35	8.2	1.89	0.145
Ref. [30]	Gap coupled	1.7	4.2	0.305	0.0069

in [29] is comparable with the proposed stub loaded CMSA configuration, but due to the three-layer stacked configuration, the volume of the antenna is larger than all the proposed gap-coupled CMSA configurations.

The antenna reported in [30] discusses a filtering antenna where arc shape patches whose angles are 90° and 180° are added around the perimeter of the circular patch. However, the antenna in [30] is quite different from the proposed configurations. The configuration referred in [30] is a filter (at port 1 and port 2) and antenna (port 3) optimized on a thinner FR4 substrate. The port 3 feed connection is a combination of the microstrip line fed directly to the annular sectoral patch which is gap-coupled to the circular patch. As against that proposed design is fabricated on a suspended FR4 substrate using the proximity feed. Further annular sectoral patches or their stub loaded variation are gap-coupled to fed circular patch. Thus structure in the proposed work may appear similar to the 'filtenna' (combined term for filter & antenna), but configuration and functionality wise, it differs.

Thus, from the above comparison, it is noted that the reported antennas which realizes wider BW or gain than the proposed configurations are either complex in their geometry, or the design methodology is missing. Although the proposed configurations employ widely reported technique, they are simpler in design than wide band MSAs obtained using slot and multi-resonator stacked configurations. They operate around the fundamental patch mode and thus offer broadside pattern characteristics. The empty area around fed patch is appropriately used to couple the compact patches to enhance the BW. Thus, simple and novel designs of gap-coupled CMSAs offering BW comparable/higher against the reported designs with smaller to comparable values of the patch size and thickness are the main technical contributions. The proposed configurations can find applications in UHF frequency band such as GPS navigation systems, satellites (L-band), pagers, Wi-Fi, and Bluetooth.

6. CONCLUSIONS

Simple and novel broadband variations of proximity fed CMSA gap-coupled with narrow annular sectoral patches, which are placed around the empty area adjoining the fed patch, are proposed. Since the proposed configuration employs multi-resonator technique using compact structures, the proposed design is simpler in implementation and yields wider BW with smaller increment in total patch size than the use of conventional half wavelength parasitic resonators. Out of all the configurations, the maximum BW of 728 MHz (55%) is achieved in CMSA gap-coupled with four pairs of annular sectors along x-axis with the gain around 9 dBi. Resonant length formulation and subsequent design methodology are presented which are useful in realizing similar antennas around TM_{11} mode of the circular patch.

REFERENCES

1. Kumar, G. and K. P. Ray, *Broadband Microstrip Antennas*, Artech House, 2003.
2. Wong, K. L., *Compact and Broadband Microstrip Antennas*, 1st Edition, John Wiley & sons, Inc., New York, USA, 2002.
3. Sun, W., Y. Li, Z. Zhang, and Z. Feng, "Broadband and low-profile microstrip antenna using strip-slot hybrid structure," *IEEE Antennas and Wireless Propagation Letters*, Vol. 16, 3118–3121, 2017.
4. Radavaram, S. and M. Pour, "Wideband radiation reconfigurable microstrip patch antenna loaded with two inverted U-slots," *IEEE Transactions on Antennas and Propagation*, Vol. 67, No. 3, 1501–1508, 2018.
5. Tiwari, R. N., P. Singh, and B. K. Kanaujia, "Butter fly shape compact microstrip antenna for wideband applications," *Progress In Electromagnetics Research*, Vol. 69, 45–50, 2017.
6. Ray, K. P. and G. Kumar, "Multi-frequency and broadband hybrid coupled circular microstrip antennas," *Electronics Letters*, Vol. 33, No. 6, 437–438, 1997.
7. Yoo, J. and H. W. Son, "A simple compact wideband microstrip antenna consisting of three staggered patches," *IEEE Antennas and Wireless Propagation Letters*, September 2020.

8. Qian, J. F., F. C. Chen, Q. X. Chu, Q. Xue, and M. J. Lancaster, "A novel electric and magnetic gap-coupled broadband patch antenna with improved selectivity and its application in MIMO system," *IEEE Transactions on Antennas and Propagation*, Vol. 66, No. 10, 5625–5629, 2018.
9. Cao, Y., Y. Cai, W. Cao, B. Xi, Z. Qian, T. Wu, and L. Zhu, "Broadband and high-gain microstrip patch antenna loaded with parasitic mushroom-type structure," *IEEE Antennas and Wireless Propagation Letters*, Vol. 18, No. 7, 1405–1409, 2019.
10. Wi, S. H., Y. S. Lee, and J. G. Yook, "Wideband microstrip patch antenna with U-shaped parasitic elements," *IEEE Transactions on Antennas and Propagation*, Vol. 55, No. 4, 1196–1199, 2007.
11. Kandwal, A. and S. K. Khah, "A novel design of gap-coupled sectoral patch antenna," *IEEE Antennas and Wireless Propagation Letters*, Vol. 12, 674–677, 2013.
12. Balaji, U., "Bandwidth enhanced circular and annular ring sectoral patch antennas," *Progress In Electromagnetics Research*, Vol. 84, 67–73, 2019.
13. Lu, H. X., F. Liu, M. Su, and Y. A. Liu, "Design and analysis of wideband U-slot patch antenna with U-shaped parasitic elements," *International Journal of RF and Microwave Computer-Aided Engineering*, Vol. 28, No. 2, 1–11, 2018.
14. Wang, Z., J. Liu, and Y. Long, "A simple wide-bandwidth and high-gain microstrip patch antenna with both sides shorted," *IEEE Antennas and Wireless Propagation Letters*, Vol. 18, No. 6, 1144–1148, 2019.
15. Sharma, V., V. K. Saxena, J. S. Saini, D. Bhatnagar, K. B. Sharma, and L. M. Joshi, "Broadband gap-coupled assembly of patches forming elliptical patch antenna," *Microwave and Optical Technology Letters*, Vol. 53, No. 2, 340–344, 2011.
16. Ding, K., C. Gao, B. Zhang, Y. Wu, and D. Qu, "A compact printed unidirectional broadband antenna with parasitic patch," *IEEE Antennas and Wireless Propagation Letters*, Vol. 16, 2341–2344, 2017.
17. Cao, Y., Y. Cai, W. Cao, Z. Qian, and L. Zhu, "Wideband microstrip patch antenna loaded with parasitic metal strips and coupling slots," *IEICE Electronics Express*, Vol. 15, No. 15, 1–8, 2018.
18. Sharma, V. and M. M. Sharma, "Wideband gap coupled assembly of rectangular microstrip patches for Wi-Max applications," *Frequenz*, Vol. 68, No. 1–2, 25–31, 2014.
19. Xu, K. D., H. Xu, Y. Liu, J. Li, and Q. H. Liu, "Microstrip patch antennas with multiple parasitic patches and shorting vias for bandwidth enhancement," *IEEE Access*, Vol. 6, 11624–11633, 2018.
20. Ray, K. P. and G. Kumar, "Multi-frequency and broadband hybrid coupled circular microstrip antennas," *Electronics Letters*, Vol. 33, No. 6, 437–438, 1997.
21. Kumar, G. and K. C. Gupta, "Broadband microstrip antennas using additional resonators gap coupled to the radiating edges," *IEEE Transaction on Antennas and Propagation*, Vol. 32, No. 12, 1375–1379, 1985.
22. Li, M., Z. Zhang, and M. C. Tang, "A compact, low-profile, wideband, electrically-controlled, tri-polarization-reconfigurable antenna with quadruple gap-coupled patches," *IEEE Transactions on Antennas and Propagation*, Vol. 68, No. 8, 6395–6400, 2020.
23. Aanandan, C. K., P. Mohanan, and K. G. Nair, "Broadband gap coupled microstrip antenna," *IEEE Transactions on Antennas and Propagation*, Vol. 38, No. 10, 1581–1586, 1990.
24. Li, H., B. Lan, J. Ding, and C. Guo, "High gain low profile wideband dual-layered substrate microstrip antenna based on multiple parasitic elements," *International Journal of Microwave and Wireless Technologies*, Vol. 10, No. 4, 453–459, 2018.
25. Chopra, R. and G. Kumar, "High gain broadband stacked triangular microstrip antennas," *Microwave and Optical Technology Letters*, 1–8, 2020.
26. Chopra, R. and G. Kumar, "Broadband and high gain multilayer multi resonator elliptical microstrip antenna," *IET Microwaves, Antennas & Propagation*, Vol. 14, No. 8, 821–829, 2020.
27. Li, D., P. Guo, Q. Dai, and Y. Fu, "Broadband capacitively coupled stacked patch antenna for GNSS applications," *IEEE Antennas and Wireless Propagation Letters*, Vol. 11, 701–704, 2012.

28. Sun, D., W. Dou, L. You, X. Yan, and R. Shen, "A broadband proximity-coupled stacked microstrip antenna with cavity-backed configuration," *IEEE Antennas and Wireless Propagation Letters*, Vol. 10, 1055–1058, 2011.
29. Katyal, A. and A. Basu, "Compact and broadband stacked microstrip patch antenna for target scanning applications," *IEEE Antennas and Wireless Propagation Letters*, Vol. 18, 381–384, 2016.
30. Sung, Y. J., "Microstrip resonator doubling as a filter and as an antenna," *IEEE Antennas and Wireless Propagation Letters*, Vol. 9, 467–470, 2010.
31. CST Microwave Studio suite, Version 2019.